

# Exactly Solvable Topological Phase Transition in a Quantum Dimer Model

Laura Shou<sup>1</sup>, Jeet Shah<sup>1,2</sup>, Matthew Lerner-Brecher<sup>3</sup>, Amol Aggarwal<sup>4</sup>, Alexei Borodin<sup>3</sup>, and Victor Galitski<sup>1</sup>

<sup>1</sup>Joint Quantum Institute, Department of Physics, University of Maryland, College Park, MD 20742, USA

<sup>2</sup>Joint Center for Quantum Information and Computer Science,

NIST/University of Maryland, College Park, MD 20742, USA

<sup>3</sup>Department of Mathematics, Massachusetts Institute of Technology, Cambridge, MA 02139, USA

<sup>4</sup>Department of Mathematics, Stanford University, Stanford, CA 94305, USA

We introduce a family of generalized Rokhsar-Kivelson (RK) Hamiltonians, which are reverse-engineered to have an arbitrary edge-weighted superposition of dimer coverings as their exact ground state at the RK point. We then focus on a quantum dimer model on the triangular lattice, with doubly-periodic edge weights. For simplicity we consider a  $2 \times 1$  periodic model in which all weights are set to one except for a tunable horizontal edge weight labeled  $\alpha$ . We analytically show that the model exhibits a continuous quantum phase transition at  $\alpha = 3$ , changing from a topological  $\mathbb{Z}_2$  quantum spin liquid ( $\alpha < 3$ ) to a columnar ordered state ( $\alpha > 3$ ). The dimer-dimer correlator decays exponentially on both sides of the transition with the correlation length  $\xi \propto 1/|\alpha - 3|$  and as a power-law at criticality. The vison correlator exhibits an exponential decay in the spin liquid phase, but becomes a constant in the ordered phase. We explain the constant vison correlator in terms of loops statistics of the double-dimer model. Using finite-size scaling of the vison correlator, we extract critical exponents consistent with the 2D Ising universality class.

*Introduction*— Quantum spin and quantum dimer models [1–7] provide complementary descriptions of strongly correlated phases of matter. In many settings there is an explicit dictionary between the two languages [8–11], with spin-singlet coverings mapped to hardcore dimers on an auxiliary lattice. Within this framework one encounters a rich landscape of phases, ranging from ordered states to a zoo of quantum spin liquids [8, 12, 13]. The latter have been an active topic of research since Anderson’s proposal of a resonating valence-bond state in the context of high- $T_c$  cuprates [14], and were later placed in a broader theoretical setting by Kitaev, Wen, and others, linking quantum spin liquids to topics as diverse as frustrated magnetism, emergent gauge theories, and topological quantum error-correcting codes [15–24]. Moreover, quantum dimer models can be realized experimentally using platforms such as Rydberg atom arrays [25–29].

Despite this broad scope, theoretical progress remains hampered by the scarcity of rigorous tools for analyzing these inherently strongly-correlated models. A notable exception is the construction by Rokhsar and Kivelson (RK) [1], which reverse-engineers a local quantum dimer Hamiltonian whose ground state at the RK point is a uniform superposition of dimer coverings, known as the RK wavefunction. At such points, equal-time correlators of diagonal operators reduce to those of a corresponding classical dimer model, allowing one to import powerful tools of classical statistical mechanics and integrable probability, including Kasteleyn’s Pfaffian technique on planar graphs [30–33] and its subsequent developments. In this work we generalize the RK construction to produce local Hamiltonians whose ground states realize *arbitrary* edge-weighted superpositions of dimer coverings on arbitrary graphs, where a standard RK Hamiltonian can be defined. This opens the door to exactly solvable models for a much wider class of spin liquids and ordered phases, as well as controlled examples of transitions between them. Furthermore, our Hamiltonian construction implies that a vast

number of results derived for classical edge-weighted dimer models [34–46] are now applicable to a corresponding edge-weighted quantum dimer model. For example, the frozen corners and multiple so-called “smooth” or “gaseous” regions seen in a  $2 \times 2$  periodic Aztec diamond will also be present in the corresponding quantum dimer model using our construction. We focus here on an analytically tractable quantum dimer model on the triangular lattice that exhibits a continuous quantum phase transition between a topological  $\mathbb{Z}_2$  spin liquid and a symmetry-broken ordered state (Fig. 1).

*Review of the RK Hamiltonian*— The quantum dimer Hilbert space is the span of the orthonormal basis  $\{|C\rangle\}$ , where  $C$  denotes a dimer configuration. The RK Hamiltonian [1], written on the square lattice, is

$$H = -J \sum_{\square} [|\uparrow\uparrow\rangle \langle \downarrow\downarrow| + \text{h.c.}] + V \sum_{\square} [|\uparrow\uparrow\rangle \langle \uparrow\uparrow| + |\downarrow\downarrow\rangle \langle \downarrow\downarrow|], \quad (1)$$

where the sum is over all plaquettes of the lattice. At the RK point, when  $J = V$ , the exact ground state is solvable and is a uniform superposition of all possible dimer configurations. However, in order to witness the rich phenomena arising in weighted classical dimer models, we seek to construct a generalized RK Hamiltonian whose ground state is a weighted superposition of all possible dimer configurations.

*Exact Hamiltonian for weighted dimer coverings*— In this section, we engineer a Hamiltonian whose exact ground state can be determined and has dimer coverings appearing with amplitudes proportional to a product of the edge weights. For simplicity, we start with the square lattice, but the construction can be generalized to any graph with an RK Hamiltonian.

Consider the square lattice and denote its set of edges by  $\mathcal{E}$ . For an edge  $e \in \mathcal{E}$  and a dimer covering  $\mathcal{C}$ , let  $d_e(\mathcal{C})$  denote the dimer number, that is,  $d_e(\mathcal{C}) = 1$  if edge  $e$  is occupied in the covering  $\mathcal{C}$ , and 0 otherwise. For each edge  $e$ , we assign

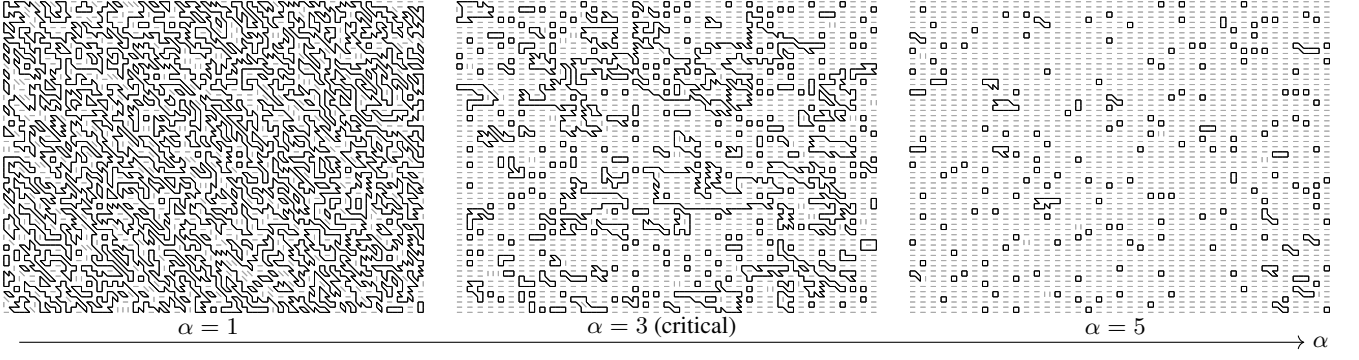


FIG. 1. The quantum dimer model on the weighted triangular lattice as given in Eq. (5) exhibits a continuous quantum phase transition as an edge weight parameter  $\alpha$  varies. Statistical behavior in the different phases and at the critical point can be seen through the behavior of random double-dimer coverings in the corresponding *classical* model, shown here for the  $2 \times 1$  periodic triangular lattice (defined in Fig. 3) with  $\alpha = 1$  (left, quantum spin liquid),  $\alpha = 3$  (center, critical), and  $\alpha = 5$  (right, columnar order), on a width 81 grid. Double-edges are shown in gray, while loops are shown in black. In the spin liquid phase  $\alpha < 3$ , the double-dimer covering forms many large macroscopic loops, while in the ordered phase  $\alpha > 3$ , there are only small loops and double edges. The ordered phase for  $\alpha > 3$  is a columnar phase with a nonzero fraction of defects. This loop behavior can be used to intuitively explain the observed vison correlator behavior in the quantum dimer model. The double-dimer coverings are generated using the Kasteleyn matrix method to compute conditional edge probabilities.

a weight  $w_e$ , which can be a complex number. The weight of a dimer covering  $W(\mathcal{C})$  is the product of the weights of all the edges that are occupied by dimers,  $W(\mathcal{C}) = \prod_{e \in \mathcal{E}} w_e^{d_e(\mathcal{C})}$ . We now construct a Hamiltonian whose ground state is

$$|\psi_{\mathbf{w}}\rangle = \sum_{\mathcal{C}} W(\mathcal{C}) |\mathcal{C}\rangle, \quad (2)$$

where  $\mathbf{w}$  is a list of weights  $w_e$ . Note that the probability of  $\mathcal{C}$  in Eq. (2) is  $|W(\mathcal{C})|^2$ , rather than  $|W(\mathcal{C})|$  which is the standard convention in edge-weighted classical dimer model literature. For convenience, we use the former convention for the general construction. Our edge-weighted RK Hamiltonian having  $|\psi_{\mathbf{w}}\rangle$  as a ground state when  $J = V$  is given by:

$$H = -J \sum_{\square} w_{p_2}^* w_{p_4}^* w_{p_1} w_{p_3} |\mathbb{I}\mathbb{I}\rangle \langle \mathbb{I}\mathbb{I}| + \text{h.c.} \\ + V \sum_{\square} |w_{p_2} w_{p_4}|^2 |\mathbb{I}\mathbb{I}\rangle \langle \mathbb{I}\mathbb{I}| + |w_{p_1} w_{p_3}|^2 |\mathbb{I}\mathbb{I}\rangle \langle \mathbb{I}\mathbb{I}|, \quad (3)$$

where the sum is over all the square plaquettes  $p$ , with  $p_i$  for  $i \in \{1, 2, 3, 4\}$  denoting the four edges of  $p$  taken in a clockwise order (see Fig. 2). For  $J = V$ , analogous to the RK

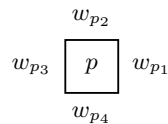


FIG. 2. A plaquette  $p$  with surrounding weights  $w_{p_1}$ ,  $w_{p_2}$ ,  $w_{p_3}$ , and  $w_{p_4}$  in a clockwise order.

point of Eq. (1), the Hamiltonian turns into a sum of (non-commuting) projectors  $H = J \sum_{\square} P_{\square}$ , where

$$P_{\square} = [w_{p_2}^* w_{p_4}^* |\mathbb{I}\mathbb{I}\rangle - w_{p_1}^* w_{p_3}^* |\mathbb{I}\mathbb{I}\rangle][w_{p_2} w_{p_4} \langle \mathbb{I}\mathbb{I}| - w_{p_1} w_{p_3} \langle \mathbb{I}\mathbb{I}|]. \quad (4)$$

It is easy to see that  $P_{\square}^2 = [|w_{p_2} w_{p_4}|^2 + |w_{p_1} w_{p_3}|^2] P_{\square}$ , implying  $P_{\square}$  is a projector up to a positive scalar factor. This immediately implies that all the eigen-energies must be non-negative. Moreover, it can be explicitly checked that  $P_{\square} |\psi_{\mathbf{w}}\rangle = 0$ , for all  $P_{\square}$ . Thus  $|\psi_{\mathbf{w}}\rangle$  is a ground state of  $H$ . Note that this construction is very general and applies to any configuration of weights, which need not be translationally invariant. It is worth noting that  $|\psi_{\mathbf{w}}\rangle$  is not necessarily the unique ground state for an arbitrary graph; however on any simply connected finite region of the square lattice, it is the unique ground state of  $H$ , as long as none of the weights are zero, since any two dimer coverings on such a region are connected by ring flips [47]. Any diagonal observable calculated in  $|\psi_{\mathbf{w}}\rangle$  will be equal to the observable calculated in a classical dimer model with covering weights proportional to  $|W(\mathcal{C})|^2$ . We can thus use results and techniques for weighted classical dimer models to draw conclusions about the quantum dimer model defined above.

*Weighted dimer Hamiltonian for the triangular lattice*— Similar to the square lattice Hamiltonian, we can write a Hamiltonian on the triangular lattice. The only modification is that we sum over several kinds of plaquettes. In order to ensure uniqueness of the ground state using ergodicity with 4 and 6-cycles [48, 49], we include larger 6-cycle plaquettes as well. The edge weights we consider on the lattice are  $2 \times 1$  periodic, i.e., they are 2-periodic in the horizontal direction and 1-periodic in the vertical direction, allowing for 6 distinct edge weights. For simplicity, we shall take one horizontal edge weight to be  $\alpha \geq 0$ , and all five other edge weights to be 1 (see Fig. 3). For these weights, the Hamiltonian using the



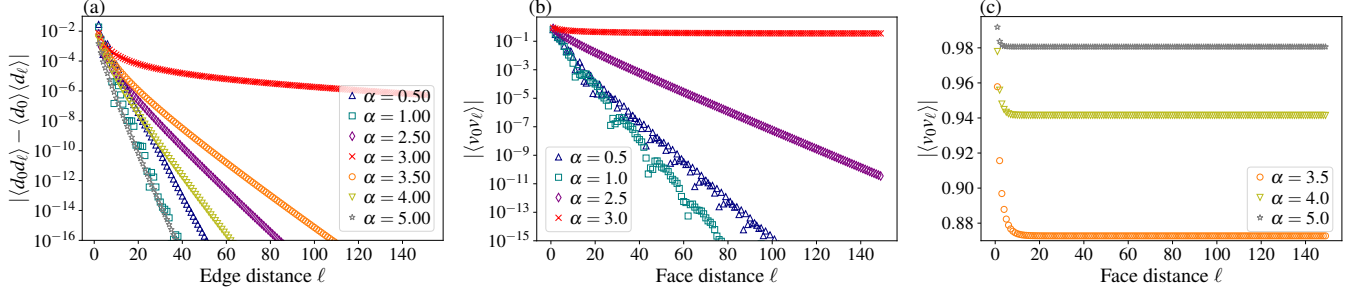


FIG. 4. Dimer-dimer and vison correlators for different values of  $\alpha$ , calculated along the path shown in Fig. 3 on a  $303 \times 303$  size grid. The path starts in the center and ends roughly midway to the boundary. (a) The dimer-dimer correlator exhibits exponential decay for all values of  $\alpha \neq 3$ , which we show analytically in the Supplemental Material [50]. (b) The vison correlator decays exponentially for  $\alpha < 3$ , signaling a spin liquid phase. It exhibits power-law decay at the critical value  $\alpha = 3$ . (c) The vison correlator is constant for  $\alpha > 3$ , identifying a trivial ordered phase. In all cases, correlators for the adjacent vertical path and a horizontal path (not shown) demonstrate similar decay or lack thereof, with some periodic differences mostly depending on the parity of the path distance.

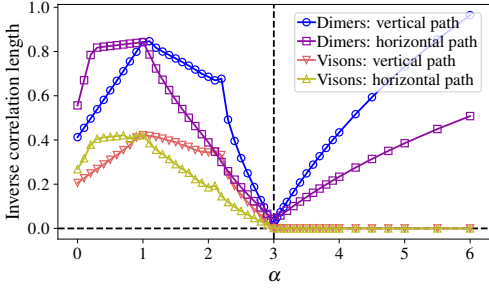


FIG. 5. Inverse correlation lengths for the dimer-dimer and vison correlators across a vertical and horizontal path for system size  $303 \times 303$ , showing linear behavior near  $\alpha = 3$ . The inverse correlation length is calculated with respect to the edge or face distance, which is half the coordinate or lattice. The labeled vertical path goes through horizontal edges with weight 1, but the values for the adjacent path through edges with weight  $\alpha$  behave similarly.

where  $I_{2|E|}$  is the  $2|E| \times 2|E|$  identity matrix,  $(K^{-1})_E$  is the restriction of  $K^{-1}$  to  $E$  (i.e. to the  $2|E|$  vertex indices associated with  $E$ ) and  $(K')_E$  is a restricted Kasteleyn matrix with nonzero entries only for edges in  $E$ .

Having defined the relevant correlators and discussed their exact expressions, we plot them numerically in Fig. 4, and summarize the quantum phases of our model as a function of the parameter  $\alpha$  as follows. For  $\alpha < 3$ , the dimer-dimer and vison correlators decay exponentially, indicating a  $\mathbb{Z}_2$  quantum spin liquid phase. For  $\alpha = 3$ , the correlators are critical. For  $\alpha > 3$ , the dimer-dimer correlator decays exponentially, but the vison correlator is constant, indicating a trivial ordered phase. The analytic derivations of the exponential decay of the dimer-dimer correlator as well as the analytic estimates of the real space Green's function correlation lengths are given in the Supplemental Material [50]. The diverging correlation lengths for the dimer-dimer and vison correlators near the transition point are shown in Fig. 5. The critical exponents  $\beta = 1/8$  and  $\nu = 1$  for the transition, which are consistent with the 2D Ising universality class, are obtained via the finite-size scaling

numerics up to lattice size  $1001 \times 1001$  in Fig. 6.

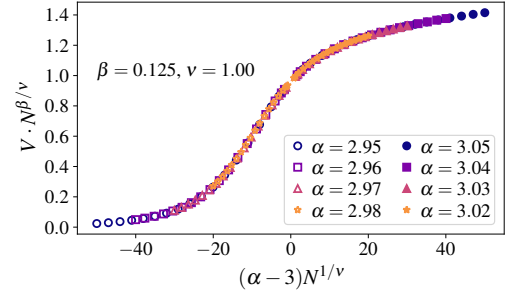


FIG. 6. Finite-size scaling for  $V = \sqrt{|\langle v_0 v_\ell \rangle|}$ , where  $|\langle v_0 v_\ell \rangle|$  is the vison correlator, at lattice distance  $\ell \sim N/4$  (halfway from the center to the edge). The path is the vertical path through weight  $\alpha$  horizontal edges starting in the center, and calculated for system sizes  $N = 41, 61, \text{ and } 101$  through  $1001$  by 60s. The curve collapse occurs for  $\beta = 1/8$  and  $\nu = 1$  as shown.

All correlator calculations are performed using the Kasteleyn matrix method (with standard floating point sparse LU methods to calculate entries of  $K^{-1}$ ), using exact expressions Eqs. (6) and (8) for the correlators. We emphasize that while we present many finite-size numerical results in this section, by Eq. (7) we also obtain exact formulas for all correlators in the infinite-size limit, which are given in terms of products and sums of explicit integrals. For example, the real space Green's function or entries of  $K^{-1}$  between two vertically separated points 0 and  $y$  in the infinite-size limit is given as:

$$\langle 0 | K^{-1} | y \rangle = \frac{\pm i}{4\pi^2} \int_0^{2\pi} \int_0^{2\pi} \frac{2 \sin(k_y) e^{-ik_y y} dk_x dk_y}{4 \sin^2 k_y + |\alpha - e^{ik_y} - e^{-ik_x} - e^{-ik_x} e^{-ik_y}|^2}, \quad (9)$$

with the sign depending on the column parity. The integral can also be turned into a single integral using contour integration. Sums and products of such integrals determine all

correlations in the infinite-size limit, including dimer-dimer and vison correlators as seen by Eqs. (6) and (8).

Using this, we analytically obtain exponential decay of dimer-dimer correlators off of the critical point, equivalent to the presence of a band gap in the fermion model. Additionally, we can analytically identify the divergence of the correlation length for  $K^{-1}$ , equivalently for the real-space Green's function in the free-fermion picture, as  $\alpha \rightarrow 3$ . As detailed in the Supplemental Material [50], we analytically obtain the Green's function correlation length along a vertical path as  $\xi_G \propto 1/|\alpha - 3|$ , as  $\alpha \rightarrow 3$ . The numerical results in Fig. 5 also show that as  $\alpha \rightarrow 3$ ,  $\xi_{\text{dimer}} \propto |\alpha - 3|^{-1}$  and  $\xi_{\text{vison}} \propto (3 - \alpha)_+^{-1}$ , where  $(x)_+ = \max(0, x)$ . For  $\alpha > 3$ , the vison correlator is constant so the correlation length is  $\infty$ . For the Green's function and dimer-dimer correlator, as  $\alpha \rightarrow \infty$ ,  $\xi_G, \xi_{\text{dimer}} \propto 1/\log \alpha \rightarrow 0$ , as dimers become more frozen. Regarding the vison correlator, we note that it may be possible to analytically investigate the constant vison correlator values using the methods of Ref. [62]. A simpler vison correlator constant was evaluated for the (uniform) RK dimer model on the square-octagon lattice in Ref. [60].

To understand the nature of the phases and explain the constant vison correlator, we consider double-dimer coverings (see Fig. 1); that is, the union  $C \cup C'$  of two independent random dimer coverings  $C, C'$ . Since each vertex will have two edges present, the double-dimer covering consists only of loops and double edges. For critical bipartite lattices, the double-dimer model is expected to behave as the Conformal Loop Ensemble  $\text{CLE}_4$  [65–67]. Here we are primarily interested in understanding the vison correlator in the non-critical spin liquid or ordered phases. The vison correlator can be expressed in terms of the double-dimer coverings  $C \cup C'$  as

$$|\langle f_0 f_\ell \rangle|^2 = \langle (-1)^{\#\text{ dimers in } C \cup C' \text{ along } \gamma} \rangle, \quad (10)$$

where  $\gamma$  is a path from face  $f_0$  to  $f_\ell$ . Since crossing a double edge does not change the dimer parity, the vison correlator can be written in terms of the number of loops in  $C \cup C'$  surrounding each endpoint of  $\gamma$ . As seen in Fig. 1, in the quantum spin liquid phase, loops are large and complicated, allowing for many changes in parity along a vison path. In contrast, in the trivial ordered phase, loops are small and not very common, appearing similar to numerical simulations of the smooth or gaseous phase of bipartite periodic lattices [35]. This sparse loop behavior can be argued to produce a constant vison correlator, as explained further in the Supplemental Material [50].

*Conclusion*— In this Letter, we generalized the quantum dimer construction of Rokhsar and Kivelson [1] to construct quantum dimer Hamiltonians whose ground state at the RK point is an arbitrary edge-weighted superposition of dimer coverings. Using this construction, we then demonstrated the existence of an exactly solvable topological phase transition in the weighted quantum dimer model on the triangular lattice, from a  $\mathbb{Z}_2$  quantum spin liquid phase to a columnar ordered phase. We used both analytical and numerical results to identify the quantum phases using the real space Green's function,

dimer-dimer correlator, and vison correlator. Furthermore, we identified critical exponents  $\beta = 1/8$  and  $\nu = 1$ , which are consistent with those of the 2D Ising universality class.

This work opens several new directions for future research on quantum phase transitions, topological phases, and statistics of dimer models. A natural question is to study the model away from the RK point, and to investigate the behavior and universality class of the phase transition there. Another direction is to develop a general theory and classification for non-bipartite dimer models, which does not yet exist in comparison to the theory for bipartite models [35]. Further study of the behavior of weighted quantum dimer models at the exactly solvable RK point is also a promising direction, in particular it would be interesting to identify all possible phases and topological orders that one can obtain with such models, for example in the direction of double semion phases investigated in Refs. [68, 69], or using the full six parameters in the  $2 \times 1$  model (or more general models).

*Acknowledgments*—J.S. and V.G. were supported by the US Army Research Office under Grant Number W911NF-23-1-024, Schwinger Foundation, and Simons Foundation. The work of Amol Aggarwal was partially supported by a Clay Research Fellowship and a Packard Fellowship for Science and Engineering. Alexei Borodin was supported by NSF grant DMS-2450323 and the Simons Investigator program.

*Data availability*—The code used is available [70].

- 
- [1] D. S. Rokhsar and S. A. Kivelson, Superconductivity and the Quantum Hard-Core Dimer Gas, *Phys. Rev. Lett.* **61**, 2376 (1988).
  - [2] R. Moessner and K. S. Raman, Quantum dimer models, in *Introduction to Frustrated Magnetism: Materials, Experiments, Theory* (Springer Berlin Heidelberg, Berlin, Heidelberg, 2011) pp. 437–479.
  - [3] R. Moessner and S. L. Sondhi, Resonating Valence Bond Phase in the Triangular Lattice Quantum Dimer Model, *Phys. Rev. Lett.* **86**, 1881 (2001).
  - [4] R. Moessner, S. L. Sondhi, and P. Chandra, Phase diagram of the hexagonal lattice quantum dimer model, *Phys. Rev. B* **64**, 144416 (2001).
  - [5] G. Misguich and F. Mila, Quantum dimer model on the triangular lattice: Semiclassical and variational approaches to vison dispersion and condensation, *Phys. Rev. B* **77**, 134421 (2008).
  - [6] A. Iosevich, D. A. Ivanov, and M. V. Feigelman, Ground-state properties of the Rokhsar-Kivelson dimer model on the triangular lattice, *Phys. Rev. B* **66**, 174405 (2002).
  - [7] T. M. Schlittler, R. Mosseri, and T. Barthel, Phase diagram of the hexagonal lattice quantum dimer model: Order parameters, ground-state energy, and gaps, *Phys. Rev. B* **96**, 195142 (2017).
  - [8] L. Balents, M. P. A. Fisher, and S. M. Girvin, Fractionalization in an easy-axis Kagome antiferromagnet, *Phys. Rev. B* **65**, 224412 (2002).
  - [9] S. Balasubramanian, V. Galitski, and A. Vishwanath, Classical vertex model dualities in a family of two-dimensional frustrated quantum antiferromagnets, *Phys. Rev. B* **106**, 195127 (2022).
  - [10] S. Balasubramanian, D. Bulmash, V. Galitski, and A. Vishwanath, Interplay of symmetry breaking and deconfinement in

- three-dimensional quantum vertex models, *Phys. Rev. B* **110**, L180401 (2024).
- [11] J. Shah, G. Nambiar, A. V. Gorshkov, and V. Galitski, A quantum monomer-dimer model on Penrose tilings (2025), [arXiv:2503.15588](https://arxiv.org/abs/2503.15588).
- [12] L. Savary and L. Balents, Quantum spin liquids: A review, *Rep. Prog. Phys.* **80**, 016502 (2017).
- [13] M. Hermele, M. P. A. Fisher, and L. Balents, Pyrochlore photons: The  $U(1)$  spin liquid in a  $S = 1/2$  three-dimensional frustrated magnet, *Phys. Rev. B* **69**, 064404 (2004).
- [14] R. Moessner and S. L. Sondhi, Ising and dimer models in two and three dimensions, *Phys. Rev. B* **68**, 054405 (2003).
- [15] A. Kitaev, Anyons in an exactly solved model and beyond, *Ann. Phys.* **321**, 2 (2006), [arxiv:cond-mat/0506438](https://arxiv.org/abs/cond-mat/0506438).
- [16] A. Kitaev, Fault-tolerant quantum computation by anyons, *Annals of Physics* **303**, 2 (2003).
- [17] X.-G. Wen, Quantum orders and symmetric spin liquids, *Phys. Rev. B* **65**, 165113 (2002).
- [18] X.-G. Wen, *Quantum Field Theory of Many-Body Systems: From the Origin of Sound to an Origin of Light and Electrons* (Oxford University Press, 2007).
- [19] M. A. Levin and X.-G. Wen, String-net condensation: A physical mechanism for topological phases, *Phys. Rev. B* **71**, 045110 (2005).
- [20] R. Moessner, S. L. Sondhi, and E. Fradkin, Short-ranged resonating valence bond physics, quantum dimer models, and Ising gauge theories, *Phys. Rev. B* **65**, 024504 (2001).
- [21] T. Senthil and M. P. A. Fisher, Fractionalization, topological order, and cuprate superconductivity, *Phys. Rev. B* **63**, 134521 (2001).
- [22] T. Senthil and M. P. A. Fisher, Fractionalization in the cuprates: Detecting the topological order, *Phys. Rev. Lett.* **86**, 292 (2001).
- [23] G. Misguich, D. Serban, and V. Pasquier, Quantum dimer model on the Kagome lattice: Solvable dimer-liquid and Ising gauge theory, *Phys. Rev. Lett.* **89**, 137202 (2002).
- [24] A. M. Essin and M. Hermele, Classifying fractionalization: Symmetry classification of gapped  $F_2$  spin liquids in two dimensions, *Phys. Rev. B* **87**, 104406 (2013).
- [25] G. Semeghini, H. Levine, A. Keesling, S. Ebadi, T. T. Wang, D. Bluvstein, R. Verresen, H. Pichler, M. Kalinowski, R. Samajdar, A. Omran, S. Sachdev, A. Vishwanath, M. Greiner, V. Vuletić, and M. D. Lukin, Probing topological spin liquids on a programmable quantum simulator, *Science* **374**, 1242 (2021).
- [26] R. Verresen, M. D. Lukin, and A. Vishwanath, Prediction of Toric Code Topological Order from Rydberg Blockade, *Phys. Rev. X* **11**, 031005 (2021).
- [27] J. Shah, G. Nambiar, A. V. Gorshkov, and V. Galitski, Quantum Spin Ice in Three-Dimensional Rydberg Atom Arrays, *Phys. Rev. X* **15**, 011025 (2025).
- [28] Z. Zeng, G. Giudici, and H. Pichler, Quantum dimer models with Rydberg gadgets, *Phys. Rev. Res.* **7**, L012006 (2025).
- [29] Z. Yan, R. Samajdar, Y.-C. Wang, S. Sachdev, and Z. Y. Meng, Triangular lattice quantum dimer model with variable dimer density, *Nat. Commun.* **13**, 5799 (2022).
- [30] P. W. Kasteleyn, The statistics of dimers on a lattice: I. the number of dimer arrangements on a quadratic lattice, *Physica* **27**, 1209 (1961).
- [31] P. W. Kasteleyn, Dimer statistics and phase transitions, *J. Math. Phys.* **4**, 287 (1963).
- [32] H. N. Temperley and M. E. Fisher, Dimer problem in statistical mechanics-an exact result, *Phil. Mag.* **6**, 1061 (1961).
- [33] M. E. Fisher, Statistical mechanics of dimers on a plane lattice, *Phys. Rev.* **124**, 1664 (1961).
- [34] H. Cohn, R. Kenyon, and J. Propp, A variational principle for domino tilings, *J. Amer. Math. Soc.* **14**, 297 (2001).
- [35] R. Kenyon, A. Okounkov, and S. Sheffield, Dimers and amoebae, *Ann. of Math. (2)* **163**, 1019 (2006).
- [36] C. Boutillier, Pattern densities in non-frozen planar dimer models, *Comm. Math. Phys.* **271**, 55 (2007).
- [37] R. Kenyon, Lectures on Dimers (2009), [arXiv:0910.3129](https://arxiv.org/abs/0910.3129).
- [38] S. Chhita, K. Johansson, and B. Young, Asymptotic domino statistics in the Aztec diamond, *Ann. Appl. Probab.* **25**, 1232 (2015).
- [39] S. Chhita and B. Young, Coupling functions for domino tilings of Aztec diamonds, *Adv. Math.* **259**, 173 (2014).
- [40] S. Chhita and K. Johansson, Domino statistics of the two-periodic Aztec diamond, *Adv. Math.* **294**, 37 (2016).
- [41] T. Berggren and M. Duits, Correlation functions for determinantal processes defined by infinite block Toeplitz minors, *Adv. Math.* **356**, 106766, 48 (2019).
- [42] M. Duits and A. B. J. Kuijlaars, The two-periodic Aztec diamond and matrix valued orthogonal polynomials, *J. Eur. Math. Soc. (JEMS)* **23**, 1075 (2021).
- [43] V. Gorin, *Lectures on random lozenge tilings*, Cambridge Studies in Advanced Mathematics, Vol. 193 (Cambridge University Press, Cambridge, 2021) pp. viii+250.
- [44] A. Borodin and M. Duits, Biased  $2 \times 2$  periodic Aztec diamond and an elliptic curve, *Probab. Theory and Relat. Fields* **187**, 259 (2023).
- [45] T. Berggren and A. Borodin, *Geometry of the doubly periodic aztec dimer model* (2025).
- [46] C. Boutillier and B. Tilière, Fock's dimer model on the Aztec diamond, [arXiv:2405.20284](https://arxiv.org/abs/2405.20284) (2025).
- [47] W. P. Thurston, Conway's tiling groups, *Amer. Math. Monthly* **97**, 757 (1990).
- [48] I. Hartarsky, L. Lichev, and F. L. Toninelli, Local dimer dynamics in higher dimensions, *Ann. Inst. Henri Poincaré Comb. Phys. Interact.* **10.4171/AIHPD/200** (2024), published online 26 August 2024.
- [49] C. Kenyon and E. Rémila, Perfect matchings in the triangular lattice, *Discrete Math.* **152**, 191 (1996).
- [50] See Supplemental Material, which includes Refs. [2, 30, 34, 35, 37, 43, 48, 49, 51, 52, 56, 60, 61, 65, 71–77].
- [51] C. L. Henley, Relaxation time for a dimer covering with height representation, *J. Statist. Phys.* **89**, 483 (1997).
- [52] E. Fradkin, D. A. Huse, R. Moessner, V. Oganesyan, and S. L. Sondhi, Bipartite Rokhsar–Kivelson points and cantor deconfinement, *Phys. Rev. B* **69**, 224415 (2004).
- [53] C. Nash and D. O'Connor, Dimer geometry, amoebae and a vortex dimer model, *J. Phys. A* **50**, 355002, 30 (2017).
- [54] E. W. Montroll, R. B. Potts, and J. C. Ward, Correlations and spontaneous magnetization of the two-dimensional Ising model, *J. Math. Phys.* **4**, 308 (1963).
- [55] R. Kenyon, Local statistics of lattice dimers, *Ann. Inst. Henri Poincaré (B) Probab. Stat.* **33**, 591 (1997).
- [56] P. Fendley, R. Moessner, and S. L. Sondhi, Classical dimers on the triangular lattice, *Phys. Rev. B* **66**, 214513 (2002).
- [57] D. B. Wilson, Determinant algorithms for random planar structures, in *SODA*, Vol. 97 (ACM/SIAM, 1997) pp. 258–267.
- [58] H. R. Lee and B. D. Saunders, Fraction free Gaussian elimination for sparse matrices, *J. Symb. Comput.* **19**, 393 (1995).
- [59] G. C. Nakos, P. R. Turner, and R. M. Williams, Fraction-free algorithms for linear and polynomial equations, *ACM SIGSAM Bull.* **31**, 11 (1997).
- [60] J. Shah, L. Shou, J. Shuler, and V. Galitski, Breakdown of the thermodynamic limit in quantum spin and dimer models, [arXiv preprint arXiv:2506.15769](https://arxiv.org/abs/2506.15769) (2025).
- [61] D. Cimasoni and N. Reshetikhin, Dimers on surface graphs and

- spin structures. I, *Comm. Math. Phys.* **275**, 187 (2007).
- [62] E. L. Basor and T. Ehrhardt, Asymptotics of block Toeplitz determinants and the classical dimer model, *Comm. Math. Phys.* **274**, 427 (2007).
- [63] E. Basor and P. Bleher, Exact solution of the classical dimer model on a triangular lattice: monomer-monomer correlations, *Comm. Math. Phys.* **356**, 397 (2017).
- [64] T. Senthil and M. P. A. Fisher,  $Z_2$  gauge theory of electron fractionalization in strongly correlated systems, *Phys. Rev. B* **62**, 7850 (2000).
- [65] R. Kenyon, Conformal invariance of loops in the double-dimer model, *Comm. Math. Phys.* **326**, 477 (2014).
- [66] J. Dubédat, Double dimers, conformal loop ensembles and isomonodromic deformations, *J. Eur. Math. Soc. (JEMS)* **21**, 1 (2019).
- [67] M. Basok and D. Chelkak, Tau-functions à la Dubédat and probabilities of cylindrical events for double-dimers and  $CLE(4)$ , *J. Eur. Math. Soc. (JEMS)* **23**, 2787 (2021).
- [68] Y. Qi, Z.-C. Gu, and H. Yao, Double-semion topological order from exactly solvable quantum dimer models, *Phys. Rev. B* **92**, 155105 (2015).
- [69] O. Buerschaper, S. C. Morampudi, and F. Pollmann, Double semion phase in an exactly solvable quantum dimer model on the kagome lattice, *Phys. Rev. B* **90**, 195148 (2014).
- [70] L. Shou, *dimers-weighted-triangular* (2026), GitHub repository.
- [71] D. Cimasoni, The geometry of dimer models, *Winter Braids Lect. Notes* **1**, Exp. No. 2, 14 (2014).
- [72] P. W. Kasteleyn, Graph theory and crystal physics, in *Graph Theory and Theoretical Physics*, edited by F. Harary (Academic Press, London, 1967) pp. 43–110.
- [73] H. Broer and F. Takens, *Dynamical systems and chaos*, Applied Mathematical Sciences, Vol. 172 (Springer, New York, 2011) pp. xvi+313.
- [74] V. I. Arnol'd, *Geometrische Methoden in der Theorie der gewöhnlichen Differentialgleichungen* (Birkhäuser Verlag, Basel, 1987) p. 320, translated from the Russian by Ernst Günter Giessmann, Bernd Graw and Horst Theel.
- [75] M. E. Fisher and J. Stephenson, Statistical mechanics of dimers on a plane lattice. II. dimer correlations and monomers, *Phys. Rev.* **132**, 1411 (1963).
- [76] R. Kenyon, Height fluctuations in the honeycomb dimer model, *Comm. Math. Phys.* **281**, 675 (2008).
- [77] C. Boutillier, D. Cimasoni, and B. de Tilière, Minimal bipartite dimers and higher genus Harnack curves, *Probab. Math. Phys.* **4**, 151 (2023).

# Exactly Solvable Topological Phase Transition in a Quantum Dimer Model

## Supplemental Material

Laura Shou <sup>1</sup>, Jeet Shah <sup>1,2</sup>, Matthew Lerner-Brecher,<sup>3</sup> Amol Aggarwal <sup>4</sup>, Alexei Borodin <sup>3</sup> and Victor Galitski<sup>1</sup>

<sup>1</sup>*Joint Quantum Institute, Department of Physics, University of Maryland, College Park, MD 20742, USA*

<sup>2</sup>*Joint Center for Quantum Information and Computer Science,  
NIST/University of Maryland, College Park, MD 20742, USA*

<sup>3</sup>*Department of Mathematics, Massachusetts Institute of Technology, Cambridge, MA 02139, USA*

<sup>4</sup>*Department of Mathematics, Stanford University, Stanford, CA 94305, USA*

In the Supplemental Material, we provide additional details, proofs, and analytical and numerical results to support the Main Text.

### CONTENTS

|  |    |
|--|----|
| I. Weighted Hamiltonian details                                      | 1  |
| II. Review of Kasteleyn's method                                     | 2  |
| III. Infinite domain limit   | 3  |
| IV. Exponential decay and correlation lengths off the critical point | 6  |
| V. Power-law decay at the critical point                             | 9  |
| VI. Critical exponents, finite-size scaling, and curve collapse      | 10 |
| VII. Double-dimer coverings and constant visons                      | 11 |
| References   | 12 |

### I. WEIGHTED HAMILTONIAN DETAILS

In this section, we provide further details for construction and ground state uniqueness of the Hamiltonian in Eq. (5) of the Main Text. Previous quantum dimer Hamiltonians on the triangular lattice typically include only unweighted 4-cycle ring flip terms. However, as observed in [S1], 4-cycle ring flips are in general not sufficient, even in planar rectangular domains, to connect two dimer coverings on the triangular lattice. Ref. [S2] showed that one can use 4, 6, and 8-cycle flips to connect any two dimer coverings on a simply connected region of the triangular lattice, and Ref. [S1] reduced this to only 4 and 6-cycle flips for rectangular domains. We use this latter result to obtain ground state uniqueness for the Hamiltonian defined in Eq. (5) of the Main Text.

First we give the general construction for the weighted projectors in the Hamiltonian for an arbitrary plaquette, although we will only need 4 and 6-cycle plaquettes. Let  $A$  be a plaquette whose boundary consists of  $2\ell$  edges  $e_1, \dots, e_{2\ell}$  traversed in order, with corresponding edge weights  $w_1, \dots, w_{2\ell}$ . Let  $|135 \dots (2\ell - 1)\rangle$  denote the dimer configurations with dimers on edges  $e_1, e_3, \dots, e_{2\ell-1}$  of  $A$ , and  $|246 \dots (2\ell)\rangle$  those with dimers on edges  $e_2, e_4, \dots, e_{2\ell}$ . Then using the notation  $\mathcal{P}(|\psi\rangle) \equiv |\psi\rangle\langle\psi|$ , we define analogously to Eq. (4) of the Main Text,

$$P_A := \mathcal{P} \{ (w_2 w_4 \cdots w_{2\ell})^* |135 \dots (2\ell - 1)\rangle - (w_1 w_3 \dots w_{2\ell-1})^* |246 \dots (2\ell)\rangle \}. \quad (\text{S1})$$

More explicitly, let  $V_{A_1}$  be the projection onto the set of dimer configurations such that  $A$  is flippable and has dimers on edges  $e_1, \dots, e_{2\ell-1}$ , and let  $V_{A_2}$  be the projection onto the set of dimer configurations such that  $A$  is flippable and has dimers on edges  $e_2, \dots, e_{2\ell}$ . Let  $F_{A_{12}}$  be the operator which flips the plaquette  $A$  from dimers on  $e_1, e_3, \dots, e_{2\ell-1}$  to dimers on  $e_2, e_4, \dots, e_{2\ell}$ , and zero otherwise, and let  $F_{A_{21}}$  be its hermitian conjugate. Then letting  $v_1 := w_1 w_3 \dots w_{2\ell-1}$  and  $v_2 := w_2 w_4 \cdots w_{2\ell}$ , one can expand  $P_A$  as

$$P_A = |v_2|^2 V_{A_1} + |v_1|^2 V_{A_2} - (v_2^* v_1 F_{A_{12}} + \text{h.c.}). \quad (\text{S2})$$

In either form, one can explicitly calculate that  $P_A^2 = (|v_1|^2 + |v_2|^2)P_A$ , which implies  $P_A \geq 0$ .

The full Hamiltonian from Eq. (5) of the Main Text, written with the 6-cycle terms, can be taken to be

$$\begin{aligned}
 H = & \sum_{\square} \mathcal{P}(|\square\rangle - |\square\rangle) + \sum_{\square} \mathcal{P}(\alpha|\square\rangle - |\square\rangle) + \sum_{\square} \mathcal{P}(\sqrt{\alpha}|\square\rangle - |\square\rangle) + \sum_{\square} \mathcal{P}(|\square\rangle - |\square\rangle) \\
 & + \sum_{\square} \mathcal{P}(|\square\rangle - \sqrt{\alpha}|\square\rangle) + \sum_{\square} \mathcal{P}(\sqrt{\alpha}|\square\rangle - |\square\rangle) + \sum_{\square} \mathcal{P}(|\square\rangle - \sqrt{\alpha}|\square\rangle) + \sum_{\square} \mathcal{P}(\sqrt{\alpha}|\square\rangle - |\square\rangle),
 \end{aligned} \tag{S3}$$

where as before, we use the notation  $\mathcal{P}(|\psi\rangle) \equiv |\psi\rangle\langle\psi|$ , and use the subscripts in the summations to indicate the types of plaquettes in each sum. The first row of (S3) is the sum over all types of 4-cycle plaquettes, while the second row is a sum over 6-cycle plaquettes. There are other alternating 6-cycle plaquettes (Fig. S1) not included in (S3), but they can be flipped with 4-cycle ring flips so do not need to appear in the Hamiltonian.

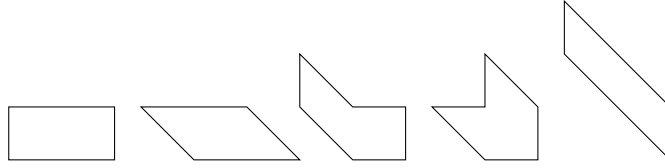


FIG. S1. Examples of alternating 6-cycle plaquettes in the triangular lattice which are flippable using 4-cycle ring flips, and thus do not need to be included in the Hamiltonian (S3).

The Hamiltonian (S3) on a rectangular domain in the triangular lattice has the unique ground state  $|\psi_w\rangle$  given by Eq. (2) of the Main Text, with the probability of  $|\mathcal{C}\rangle$  given by the classical weighted probability of the configuration  $\mathcal{C}$ . To see the above, first note that  $H \geq 0$  since  $P_A \geq 0$  for every projection term in (S3), and that  $H|\psi_w\rangle = 0$  since one can check  $P_A|\psi_w\rangle = 0$ . For uniqueness, consider a general state  $|\psi\rangle = \sum_{\mathcal{C}} a_{\mathcal{C}}|\mathcal{C}\rangle$  for coefficients  $a_{\mathcal{C}} \in \mathbb{C}$  and dimer configurations  $\mathcal{C}$ , and note that a ground state must satisfy  $P_A|\psi\rangle = 0$  for every projection term in (S3). Using ergodicity with 4 and 6-cycles from Ref. [S1], imposing  $P_A|\psi\rangle = 0$  then determines all coefficients  $a_{\mathcal{C}}$  starting from a single one of these coefficients, implying the ground state must be unique.

More generally, for any simply connected domain in the triangular lattice, one can ensure ground state uniqueness by adding in the 8-cycle terms to the Hamiltonian, using the result of Ref. [S2].

## II. REVIEW OF KASTELEYN'S METHOD

In this section, we briefly review the Kasteleyn matrix and some of its properties. For further references, see e.g. Refs. [S3–S6]. For a planar graph, one can always define a Kasteleyn orientation [S3, S5, S7, S8], which can be defined as an assignment of directions to the edges so that the number of edges oriented counterclockwise around each face is odd [S9]. For each directed edge  $(v_1 \rightarrow v_2)$  between two vertices in the graph, we assign a positive orientation if it agrees with the Kasteleyn orientation and a negative orientation if it disagrees. Recall we consider edge weights  $w(v_1, v_2) = w(v_2, v_1)$  assigned to the edges of the graph. The Kasteleyn matrix  $K$  is a weighted, signed adjacency matrix which can be defined as:

$$K(v_1, v_2) = \begin{cases} w(v_1, v_2), & (v_1 \rightarrow v_2) \text{ has positive orientation} \\ -w(v_1, v_2) & (v_1 \rightarrow v_2) \text{ has negative orientation} \\ 0, & (v_1, v_2) \text{ is not an edge} \end{cases} \tag{S4}$$

Note that  $K$  is skew-symmetric. If the graph is bipartite, then  $K$  has a block structure and one can instead consider half-size Kasteleyn matrices where the rows and columns are indexed by one of the two sets of vertices. Since we work on the triangular lattice, we will however have to use the full size matrix defined in (S4).

For a dimer configuration  $\mathcal{C}$ , the weight  $\mathcal{W}(\mathcal{C}) = \prod_{e \in \mathcal{E}} w_e^{d_e(\mathcal{C})}$  is the product of all edge weights of dimers in  $\mathcal{C}$ . By construction of the Kasteleyn orientation, the partition function can be written as [S3]

$$Z \equiv \sum_{\mathcal{C}} \mathcal{W}(\mathcal{C}) = |\text{Pf}(K)|, \tag{S5}$$

where  $\text{Pf}(K)$  denotes the Pfaffian, defined for a  $2n \times 2n$  skew-symmetric matrix  $A$  as

$$\text{Pf}(A) = \frac{1}{2^n n!} \sum_{\sigma \in S_{2n}} \text{sgn}(\sigma) \prod_{i=1}^n A_{\sigma(2i-1), \sigma(2i)}. \quad (\text{S6})$$

The Pfaffian is related to the determinant as

$$\text{Pf}(A)^2 = \det A. \quad (\text{S7})$$

Since the Pfaffian of a Kasteleyn matrix counts weighted dimer coverings for the corresponding graph, it can be used to calculate dimer probabilities and correlations. To count the number of dimer configurations where a certain set of edges  $E = \{e_1, \dots, e_k\}$ ,  $e_i = (v_i, u_i)$ , appear, one takes the Pfaffian of the Kasteleyn matrix for the subgraph with all vertices  $V_E = \{v_1, u_1, v_2, u_2, \dots, v_k, u_k\}$  (and their attached edges) removed. This leads to the Pfaffian form of Kenyon's formula [S10], [S11, §6.3],

$$\mathbb{P}[e_1, \dots, e_k \text{ all occur in a dimer covering}] = (-1)^k \left[ \prod_{i=1}^k K(v_i, u_i) \right] \text{Pf}(K_{V_E}^{-1}), \quad (\text{S8})$$

where the Pfaffian is over the  $2|E| \times 2|E|$  submatrix of  $K^{-1}$  corresponding to the  $2|E|$  vertices in  $V_E$ . The product  $\prod_{i=1}^k K(v_i, u_i)$  is just a signed product of the weights for the edges in  $E$ .

As an example, (S8) gives the dimer-dimer correlator between dimers  $\mu = (\mu_0, \mu_1)$  and  $\nu = (\nu_0, \nu_1)$  as

$$\langle d_\mu d_\nu \rangle - \langle d_\mu \rangle \langle d_\nu \rangle = K(\mu_0, \mu_1) K(\nu_0, \nu_1) [-K^{-1}(\mu_0, \nu_0) K^{-1}(\mu_1, \nu_1) + K^{-1}(\mu_0, \nu_1) K^{-1}(\mu_1, \nu_0)]. \quad (\text{S9})$$

Note this formula has an additional term compared to the bipartite case, where the dimer-dimer correlator is proportional to a single product of the Green's function at two points [S12]. Equation (S8) is also used to derive the vison correlator expression (9) in the Main Text following [S13, §II.B] and using (S7).

Kasteleyn's method can also be used to count dimer configurations on the torus using four Pfaffians [S3], which we will use in the next section.

### III. INFINITE DOMAIN LIMIT

In this section, we analytically derive the double integral formulas for  $K^{-1}$  in the infinite domain periodic limit. For the general 6-parameter model on the triangular lattice (Fig. S2), we use this to show that there is exponential decay of the dimer-dimer correlator off of the set where one of the horizontal or diagonal edge weights is equal to the sum of the other three remaining such weights (Theorem 2). The general method is similar to that of the bipartite case [S6, S12, S14], using block diagonalization of the Kasteleyn matrix. In this section, to avoid confusion with a complex parameter  $w \in \mathbb{C}$ , we will use  $W(e)$  to represent the weight of an edge  $e$ .

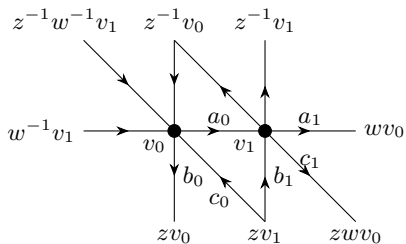


FIG. S2. Fundamental domain for the 6-parameter  $2 \times 1$  periodic triangular lattice. The horizontal weights are  $a_0$  and  $a_1$ , vertical weights are  $b_0$  and  $b_1$ , and diagonal weights are  $c_0$  and  $c_1$ . As in the Main Text, horizontal and vertical translates of the fundamental domain are indexed by variables  $w, z \in \mathbb{C}$ .

We start in the general setting of a graph, which may be non-bipartite, on the torus. Considering periodic boundary conditions, or a graph  $G$  on the torus, the partition function is given by a linear combination of four Pfaffians [S3]. There are four Kasteleyn matrices  $K^{\alpha\beta}$  with  $\alpha, \beta \in \{0, 1\}$ , defined by constructing the usual Kasteleyn matrix and then flipping the sign on horizontal

( $\alpha = 1$ ) and/or vertical ( $\beta = 1$ ) edges that wrap around the boundaries. There are then  $s_{\alpha\beta} \in \{-1, 1\}$  such that the partition function is given by

$$Z(G) = \frac{1}{2} [s_{00} \text{Pf}(K^{00}) + s_{01} \text{Pf}(K^{01}) + s_{10} \text{Pf}(K^{10}) + s_{11} \text{Pf}(K^{11})]. \quad (\text{S10})$$

It was shown in [S11] that the following formula for the correlations holds: Letting  $V_E = \{u_1, v_1, \dots, u_k, v_k\}$  be a set of vertices in  $G$ , then

$$\mathbb{E}[\mathbf{1}_{u_1 v_1} \cdots \mathbf{1}_{u_k v_k}] = \frac{(-1)^k}{Z(G)} \sum_{\alpha\beta} s_{\alpha\beta} \text{Pf}(K^{\alpha\beta}) \text{Pf}((K^{\alpha\beta})_{V_E}^{-1}) \prod_{i=1}^k \epsilon_{\alpha\beta}(u_i, v_i) w(u_i, v_i), \quad (\text{S11})$$

where  $A_E$  denotes the restriction of the matrix  $A$  to rows and columns with indices in  $E$ , and  $\epsilon_{\alpha\beta}(u_\ell, v_\ell)$  denotes the  $\alpha\beta$ -Kasteleyn orientation of the directed edge  $(u_\ell, v_\ell)$ ; i.e.  $\epsilon_{\alpha\beta}(u_\ell, v_\ell) = 1$  if edge  $(u_\ell, v_\ell)$  aligns with the  $\alpha\beta$ -Kasteleyn orientation,  $\epsilon_{\alpha\beta}(u_\ell, v_\ell) = -1$  if the edge is in the opposite orientation, and 0 otherwise.

Now suppose  $\Gamma$  is a  $\mathbb{Z}^2$ -periodic planar graph, and let  $\Gamma_{mn} = \Gamma/(m\mathbb{Z} \times n\mathbb{Z})$ , which we will view as a graph embedded in the torus. We will assume that the edges of  $\Gamma$  have a positive doubly periodic weight function  $w$ , and that  $(m, n)$  are chosen compatible with the periods. Select a fundamental domain  $\Gamma_{mn}^{0,0}$  for  $\Gamma_{mn}$  (for example, see Fig. S2 for a fundamental domain for the  $2 \times 1$  periodic triangular lattice) and let  $\Gamma_{mn}^{i,j}$  be the translate of  $\Gamma_{mn}^{0,0}$  by  $(i, j)$ . Similarly, for a point  $u \in \Gamma_{mn}^{0,0}$  in the fundamental domain, we will let  $u^{i,j}$  denote its translate by  $(i, j)$ .

For  $\alpha, \beta \in \{0, 1\}$ , let  $W^{\alpha\beta}$  be the block 2D Fourier matrix indexed by vertices of  $\Gamma_{mn}$  defined as

$$\langle u^{i,j} | W^{\alpha\beta} | v^{k,\ell} \rangle = \begin{cases} \frac{1}{\sqrt{mn}} \omega^{(2i+\alpha)k} \zeta^{(2j+\beta)\ell}, & u = v \\ 0, & \text{otherwise} \end{cases}, \quad (\text{S12})$$

where  $\omega = e^{\pi i/m}$ ,  $\zeta = e^{\pi i/n}$  are the  $(2m)$ th and  $(2n)$ th roots of unity respectively. Let  $K_{mn}^{\alpha\beta}$ ,  $\alpha, \beta \in \{0, 1\}$ , be the four Kasteleyn matrices for  $\Gamma_{mn}$  on the torus.

**Lemma 1** (block diagonalization). *The matrix*

$$L = W^{\alpha\beta} K_{mn}^{\alpha\beta} (W^{\alpha\beta})^{-1} \quad (\text{S13})$$

is block diagonal with respect to the partitioning of  $\Gamma_{mn}$  into subsets  $\Gamma_{mn}^{i,j}$ . Furthermore, the diagonal block corresponding to  $\Gamma_{mn}^{i,j}$  is given by  $L_{\omega^{2i+\alpha}, \zeta^{2j+\beta}}$  where

$$\langle u | L_{w,z} | v \rangle = \sum_{i'=-1}^1 \sum_{j'=-1}^1 w^{i'} z^{j'} \langle u^{i',j'} | K_{mn}^{00} | v \rangle. \quad (\text{S14})$$

*Proof.* Let  $u, v \in \Gamma_{mn}^{0,0}$  be points in the fundamental domain. Then for all  $i, k \in \{0, \dots, m-1\}$  and  $j, \ell \in \{0, \dots, n-1\}$ , one has

$$\langle u^{i,j} | W^{\alpha\beta} K_{mn}^{\alpha\beta} (W^{\alpha\beta})^{-1} | v^{k,\ell} \rangle = \frac{1}{mn} \sum_{i',k'=0}^{m-1} \sum_{j',\ell'=0}^{n-1} \omega^{(2i+\alpha)i'-(2k+\alpha)k'} \zeta^{(2j+\beta)j'-(2\ell+\beta)\ell'} \langle u^{i',j'} | K_{mn}^{\alpha\beta} | v^{k',\ell'} \rangle. \quad (\text{S15})$$

Consider all terms in the sum corresponding to a  $\mathbb{Z}^2$  translate of a pair  $(u^{i',j'}, v^{k',\ell'})$ ; i.e. where  $(i', j')$  and  $(k', \ell')$  are both shifted by some  $(r, s) \in \mathbb{Z}^2$  (and taken modulo  $m\mathbb{Z} \times n\mathbb{Z}$ ). The value of

$$\omega^{\alpha(i'-k')} \zeta^{\beta(j'-\ell')} \langle u^{i',j'} | K_{mn}^{\alpha\beta} | v^{k',\ell'} \rangle \quad (\text{S16})$$

will be constant across all such translates; the only place of concern is if the translate crosses the border of the domain, but then  $\omega^{\alpha(i'-k')} \zeta^{\beta(j'-\ell')}$  will undergo the same sign change as the element of the Kasteleyn matrix. The remaining portion of the terms in (S15) which changes across these translates is then

$$\omega^{2(ii'-kk')} \zeta^{2(jj'-\ell\ell')}.$$

Since the sum over the translates of this expression is 0 unless  $i = k$  and  $j = \ell$ , it follows that  $W^{\alpha\beta} K_{mn}^{\alpha\beta} (W^{\alpha\beta})^{-1}$  is indeed block diagonal.

To obtain (S14), note that when  $i = k$  and  $j = \ell$ , each term in the sum in (S15) is invariant with respect to  $\mathbb{Z}^2$  translations of  $(i', j')$  and  $(k', \ell')$  together, and thus

$$\langle u^{i,j} | W^{\alpha\beta} K_{mn}^{\alpha\beta} (W^{\alpha\beta})^{-1} | v^{i,j} \rangle = \sum_{i'=0}^{m-1} \sum_{j'=0}^{n-1} \omega^{(2i+\alpha)i'} \zeta^{(2j+\beta)j'} \langle u^{i',j'} | K_{mn}^{\alpha\beta} | v \rangle. \quad (\text{S17})$$

Since  $v \in \Gamma_{mn}^{0,0}$ , the Kasteleyn matrix entry can only be nonzero for  $i' \in \{0, 1, m-1\}$  and  $j' \in \{0, 1, n-1\}$ . As the signs in the  $i' = m-1$  or  $j' = n-1$  cases cancel with those arising from the orientation  $\epsilon_{\alpha\beta}$ , this is precisely the desired expression.  $\square$

**Corollary 1** (finite domain expressions). *Let  $L_{w,z}$  be defined as in (S14) and set  $P(w, z) = \det L_{w,z}$ , which is the characteristic polynomial. Then*

$$\det K_{mn}^{\alpha\beta} = \prod_{i=1}^{m-1} \prod_{j=1}^{n-1} P(\omega^{2i+\alpha}, \zeta^{2j+\beta}), \quad (\text{S18})$$

where  $\omega, \zeta$  are  $(2m)$ th,  $(2n)$ th roots of unity respectively. Furthermore,

$$\langle u^{i,j} | (K_{mn}^{\alpha\beta})^{-1} | v^{k,\ell} \rangle = \frac{1}{mn} \sum_{s=0}^{m-1} \sum_{t=0}^{n-1} \omega^{-(2s+\alpha)(i-k)} \zeta^{-(2t+\beta)(j-\ell)} \langle u | L_{\omega^{2s+\alpha}, \zeta^{2t+\beta}}^{-1} | v \rangle. \quad (\text{S19})$$

**Theorem 1** (infinite domain limit). *Let  $L_{w,z}$  be defined as in Corollary 1, and let  $\mathbb{T}^1$  be the unit circle in  $\mathbb{C}$ . Then as  $m, n \rightarrow \infty$ , each  $(K_{mn}^{\alpha\beta})^{-1}$  converges elementwise to  $K^{-1}$  given by*

$$\langle u^{i,j} | K^{-1} | v^{k,\ell} \rangle = -\frac{1}{4\pi^2} \int_{\mathbb{T}^1} \int_{\mathbb{T}^1} \langle u | L_{w,z}^{-1} | v \rangle w^{-(i-k)} z^{-(j-\ell)} \frac{dw}{w} \frac{dz}{z}. \quad (\text{S20})$$

Additionally, for edges  $e_1 = (u_1, v_1), \dots, e_k = (u_k, v_k)$ , letting  $V_E = \{u_1, v_1, \dots, u_k, v_k\}$ ,

$$\lim_{m,n \rightarrow \infty} \mathbb{E}[\mathbf{1}_{e_1} \cdots \mathbf{1}_{e_k}] = (-1)^k \left( \prod_{i=1}^k \epsilon_{00}(u_i, v_i) W(u_i, v_i) \right) \text{Pf}(K^{-1})_{V_E}. \quad (\text{S21})$$

*Proof.* For (S20), note that the right side of (S19) is a Riemann sum converging to the expression in (S20) for  $\langle u^{i,j} | K^{-1} | v^{k,\ell} \rangle$ . For (S21), note that for sufficiently large domains  $\Gamma_{mn}$ , we may use (S11) with  $\epsilon_{\alpha\beta}$  replaced by  $\epsilon_{00}$  since none of the selected edges will cross the boundaries of the domain. Then we have for sufficiently large  $m, n$ ,

$$\mathbb{E}[\mathbf{1}_{e_1} \cdots \mathbf{1}_{e_k}] = (-1)^k \sum_{\alpha\beta} \frac{s_{\alpha\beta} \text{Pf}(K_{mn}^{\alpha\beta})}{Z_{mn}} \text{Pf}((K_{mn}^{\alpha\beta})_E^{-1}) \prod_{i=1}^k \epsilon_{00}(u_i, v_i) W(u_i, v_i). \quad (\text{S22})$$

The coefficients  $\frac{s_{\alpha\beta} \text{Pf}(K_{mn}^{\alpha\beta})}{Z_{mn}}$  are bounded and sum to one by (S10). Then using (S20) gives (S21).  $\square$

We now specialize to the  $2 \times 1$  periodic triangular lattice, whose fundamental domain is drawn in Fig. S2.

**Theorem 2** (dimer-dimer correlator for the  $2 \times 1$  triangular lattice). *Consider the  $2 \times 1$  periodic triangular lattice  $\Gamma$  whose fundamental domain is drawn in Fig. S2. Let  $e_1, e_2$  be two edges in  $\Gamma$ , and let  $d_e$  be the dimer occupation number of the edge  $e$ . Define  $e^{r,s}$  the edge  $(r, s) + e_2$ . If none of the weights  $a_0, a_1, c_0, c_1$  are a sum of the other three, then the dimer-dimer correlator between edges  $e_1$  and  $e_2^{r,s}$  decays exponentially as  $|r|, |s| \rightarrow \infty$ .*

*Proof.* From the fundamental domain drawn in Fig. S2, we can read off the matrix  $L_{w,z}$  as

$$L_{w,z} = \begin{bmatrix} b_0(z - z^{-1}) & a_0 - a_1 w^{-1} - c_0 z - c_1 (wz)^{-1} \\ -a_0 + a_1 w + c_0 z^{-1} + c_1 wz & -b_1(z - z^{-1}) \end{bmatrix}, \quad (\text{S23})$$

and thus

$$P(w, z) \equiv \det L_{w,z} = -b_0 b_1 (z - z^{-1})^2 + (a_0 - a_1 w^{-1} - c_0 z - c_1 (wz)^{-1})(a_0 - a_1 w - c_0 z^{-1} - c_1 wz). \quad (\text{S24})$$

For  $w, z \in \mathbb{T}^1$ , both terms in the sum above are equal to the magnitude squared of a complex number. Thus  $P(w, z)$  can only vanish if both complex numbers vanish, which corresponds precisely to the case when one of  $a_0, a_1, c_0, c_1$  is a sum of the other

three. Consequently, if this condition does not hold, then for any choice of  $u, v$ ,  $L_{w,z}^{-1}(u, v)$  is a smooth and bounded function over  $w, z \in \mathbb{T}^1$ .

Now, let  $e_1 = (u_1, v_1)$  and  $e_2 = (u_2, v_2)$ . By Eq. (S21) of Theorem 1, the dimer-dimer correlator is given by

$$\text{Cov}(d_{e_1}, d_{e_2^{r,s}}) = \left( \prod_{i=0}^1 \epsilon_{00}(u_i, v_i) W(u_i, v_i) \right) [\text{Pf}(K^{-1})_{V_E} - \text{Pf}(K^{-1})_{V_{E_1}} \text{Pf}(K^{-1})_{V_{E_2}}], \quad (\text{S25})$$

where  $V_{E_1} = \{u_1, v_1\}$ ,  $V_{E_2} = \{u_2^{r,s}, v_2^{r,s}\}$ , and  $V_E = V_{E_1} \cup V_{E_2}$ . Expanding out the Pfaffians one gets

$$\text{Pf}(K^{-1})_{V_E} - \text{Pf}(K^{-1})_{V_{E_1}} \text{Pf}(K^{-1})_{V_{E_2}} = -K^{-1}(u_1, u_2^{r,s})K^{-1}(v_1, v_2^{r,s}) + K^{-1}(u_1, v_2^{r,s})K^{-1}(v_1, u_2^{r,s}).$$

The function  $L_{w,z}^{-1}(u, v)$  is a ratio of trigonometric polynomials and is analytic when  $P(w, z)$  has no zeros. Since the formula (S20) for  $K^{-1}$  is a Fourier transform of  $\langle u | L_{w,z}^{-1} | v \rangle$ , a Paley–Wiener theorem implies these terms and the above correlator decay exponentially in  $r, s$ .  $\square$

#### IV. EXPONENTIAL DECAY AND CORRELATION LENGTHS OFF THE CRITICAL POINT

In this section, we consider the  $2 \times 1$  periodic triangular lattice with one horizontal edge weight  $\alpha$ , and the other five edge weights equal to one. We first explicitly write the formulas from the previous section in this case, and then use contour integration and a Paley–Wiener theorem to analytically study the correlation length of  $K^{-1}$  along a vertical path as  $\alpha \rightarrow 3$ . We also compare to numerical plots of the correlation lengths.

To obtain the explicit formulas for the double integrals, we start from (S23) which gives the magnetic Kasteleyn matrix

$$L_{w,z} = \begin{bmatrix} z - z^{-1} & \alpha - z - w^{-1} - z^{-1}w^{-1} \\ -\alpha + w + z^{-1} + zw & -(z - z^{-1}) \end{bmatrix}. \quad (\text{S26})$$

The inverse is

$$L_{w,z}^{-1} = \frac{1}{P(w, z)} \begin{bmatrix} -(z - z^{-1}) & -\alpha + z + w^{-1} + z^{-1}w^{-1} \\ \alpha - w - z^{-1} - zw & z - z^{-1} \end{bmatrix}, \quad (\text{S27})$$

where  $P(w, z) = \det L_{w,z} = -(z - z^{-1})^2 + (\alpha - z - w^{-1} - z^{-1}w^{-1})(\alpha - w - z^{-1} - zw)$  is the *characteristic polynomial*. When  $w = e^{ik_x}$  and  $z = e^{ik_y}$  are on the unit circle, this gives

$$P(e^{ik_x}, e^{ik_y}) = 4 \sin^2 k_y + |\alpha - e^{ik_y} - e^{-ik_x} - e^{-ik_x} e^{-ik_y}|^2, \quad (\text{S28})$$

which is also the product of band dispersions for the corresponding free-fermion model.

We now index vertices in the triangular lattice by coordinates  $(x, y, t)$ , where  $(x, y) \in \mathbb{Z}^2$  denotes the translation of the fundamental cell, and  $u, v \in \{0, 1\}$  specifies the vertex  $v_0$  or  $v_1$  in Fig. S2 or in Fig. 3 of the Main Text. Then in the infinite size periodic limit, (S27) and Theorem 1 imply

$$\langle 0, 0, u | K^{-1} | x, y, v \rangle = \int_0^{2\pi} \int_0^{2\pi} \frac{Q_{uv}(e^{ik_x}, e^{ik_y}) e^{-i(k_x x + k_y y)}}{4 \sin^2 k_y + |\alpha - e^{ik_y} - e^{-ik_x} - e^{-ik_x} e^{-ik_y}|^2} \frac{dk_x}{2\pi} \frac{dk_y}{2\pi}, \quad (\text{S29})$$

where  $Q_{uv}(w, z)$  is the rational function given by the  $(u, v)$  matrix entries [without  $1/P(w, z)$ ] of (S27).

To study exponential decay and correlation lengths analytically, we consider the infinite size periodic limit as in the previous section. The matrix elements of  $K^{-1}$  given in Eq. (S29) correspond to the 2D Fourier transform of a rational function  $F$  whose denominator is given by the product of band dispersions  $P(e^{ik_x}, e^{ik_y})$  in Eq. (S28). As in Theorem 2, using that  $P(e^{ik_x}, e^{ik_y})$  is a sum of two nonnegative terms, we see it can only be zero if  $k_y = k_x = 0$  and  $\alpha = 3$ . In particular, for  $\alpha \neq 3$ , there is a band gap since  $P(e^{ik_x}, e^{ik_y}) \neq 0$  for all  $k_x, k_y \in [0, 2\pi]$ , and as follows in Theorem 2, analyticity of the resulting function  $F$  implies exponential decay of its Fourier transform, and hence of the matrix elements of  $K^{-1}$ . As a result, we know from the above argument expressed in Theorem 2 that the dimer-dimer connected correlator decays exponentially for  $\alpha \neq 3$ ,

$$|\langle d_\mu d_\nu \rangle - \langle d_\mu \rangle \langle d_\nu \rangle| \leq C e^{-c \text{dist}(\mu, \nu)}, \quad (\text{S30})$$

where  $C, c$  may depend on  $\alpha$ , and  $\text{dist}(\mu, \nu)$  denotes some distance (such as Euclidean distance) on the lattice.

Next, for  $\alpha \neq 3$ , we calculate the correlation length  $\xi_G$  for the inverse Kasteleyn limit, which corresponds to the real-space Green's function in the corresponding free-fermion model, along a vertical path. We start with the infinite size periodic limit formula (S29), which gives expressions of the form

$$\int_0^{2\pi} \int_0^{2\pi} \frac{e^{ij k_x} e^{i\ell k_y}}{4 \sin^2 k_y + |\alpha - e^{ik_y} - e^{-ik_x} - e^{-ik_x} e^{-ik_y}|^2} \frac{dk_x}{2\pi} \frac{dk_y}{2\pi} = \frac{1}{(2\pi i)^2} \oint_{S^1} \oint_{S^1} \frac{w^j z^\ell}{c_1(z, \alpha) w^2 + c_2(z, \alpha) w + c_3(z, \alpha)} dw \frac{dz}{z}, \quad (\text{S31})$$

where

$$\begin{aligned} c_1(z, \alpha) &= (z - \alpha)(z + 1) \\ c_2(z, \alpha) &= 5 + \alpha^2 - (z^2 + z^{-2}) + (1 - \alpha)(z + z^{-1}) \\ c_3(z, \alpha) &= (z^{-1} - \alpha)(z^{-1} + 1) \end{aligned} \quad (\text{S32})$$

The denominator of the integrand factors as  $c_1(z, \alpha)w^2 + c_2(z, \alpha)w + c_3(z, \alpha) = c_1(z, \alpha)[w - r_+(z, \alpha)][w - r_-(z, \alpha)]$  for

$$r_\pm(z, \alpha) = \frac{-c_2(z, \alpha) \pm \sqrt{c_2(z, \alpha)^2 - 4c_1(z, \alpha)c_3(z, \alpha)}}{2c_1(z, \alpha)}, \quad (\text{S33})$$

for  $z \neq -1, \alpha$  [S15]. For  $z = e^{ik_y}$  with  $k_y \in \mathbb{R}$ , we have

$$|r_+(z, \alpha)r_-(z, \alpha)| = \frac{|c_2(z, \alpha)^2 - (c_2(z, \alpha)^2 - 4c_1(z, \alpha)c_3(z, \alpha))|}{4|c_1(z, \alpha)|^2} = \frac{|c_3(z, \alpha)|}{|c_1(z, \alpha)|} = 1. \quad (\text{S34})$$

Also,  $c_2(e^{ik_y}, \alpha)$  is real and is  $> 0$ , so we see that  $|r_+(e^{ik_y}, \alpha)| \leq |r_-(e^{ik_y}, \alpha)|$ . We know there are no zeros of the denominator of the integrand in (S31) for any  $|z| = |w| = 1$  iff  $\alpha \neq 3$ . Thus for  $\alpha \neq 3$ , we must have  $|r_+(z, \alpha)| < 1$  and  $|r_-(z, \alpha)| > 1$  for all  $|z| = |w| = 1$ . Therefore, for  $j \geq 0$  and  $\alpha \neq 3$ , the only pole inside the unit circle is at  $w = r_+(z, \alpha)$ , and the residue theorem implies

$$\begin{aligned} \frac{1}{(2\pi i)^2} \oint_{S^1} \frac{z^\ell dz}{z} \oint_{S^1} \frac{w^j}{c_1(z, \alpha)[w - r_+(z, \alpha)][w - r_-(z, \alpha)]} dw &= \int_0^{2\pi} \frac{[r_+(e^{ik_y}, \alpha)]^j e^{i\ell k_y}}{c_1(z, \alpha)[r_+(e^{ik_y}, \alpha) - r_-(e^{ik_y}, \alpha)]} \frac{dk_y}{2\pi} \\ &= \int_0^{2\pi} \frac{[r_+(e^{ik_y}, \alpha)]^j e^{i\ell k_y}}{\sqrt{c_2(e^{ik_y}, \alpha)^2 - 4c_1(e^{ik_y}, \alpha)c_3(e^{ik_y}, \alpha)}} \frac{dk_y}{2\pi}. \end{aligned} \quad (\text{S35})$$

We consider the decay along a vertical path in the triangular lattice. For example, we can consider fixed  $j \geq 0$ , and replace  $e^{i\ell k_y}$  in the numerator with  $\sin(k_y)e^{i\ell k_y}$ ; up to constant factors this corresponds to the Green's function between two points separated vertically. The integral (S35), with modified numerator, is then the Fourier transform of the function

$$f_a(k_y) = \frac{2 \sin(k_y) c_1(e^{ik_y}, \alpha) [r_+(e^{ik_y}, \alpha)]^j}{\sqrt{c_2(e^{ik_y}, \alpha)^2 - 4c_1(e^{ik_y}, \alpha)c_3(e^{ik_y}, \alpha)}}, \quad (\text{S36})$$

for  $k_y \in \mathbb{R}/(2\pi\mathbb{Z})$ . The rate of decay of the Fourier transform of  $f_a$  is determined by the nearest complex zero of  $f_a$ , due to a Paley–Wiener theorem:

**Lemma 2.** *If  $f$  is  $2\pi$ -periodic and real analytic with analytic extension to a neighborhood of the strip  $\{z \in \mathbb{C} : |\text{Im } z| \leq \kappa\}$  for some  $\kappa > 0$ , then the Fourier coefficients  $\hat{f}(\xi) = \frac{1}{2\pi} \int_0^{2\pi} f(x) e^{-i\xi x} dx$  satisfy*

$$|\hat{f}(\xi)| \leq C e^{-\kappa|\xi|}, \quad (\text{S37})$$

for some constant  $C = C(f)$ . Conversely, if the Fourier coefficients have the above exponential decay, then  $f$  has analytic extension to the strip  $\{z \in \mathbb{C} : |\text{Im } z| < \kappa\}$ .

More generally, a  $d$ -dimensional version can be formulated, see for example, Ref. [S16, Lemma 5.6], [S17].

Therefore to determine the inverse correlation length of  $K^{-1}$ , we locate the zeros of

$$d(e^{ik_y}, \alpha) := \sqrt{c_2(e^{ik_y}, \alpha)^2 - 4c_1(e^{ik_y}, \alpha)c_3(e^{ik_y}, \alpha)},$$

for  $k_y = t + is$  which are closest to the real line.

When  $\alpha = 3$ , we see that  $k_y = 0$  solves  $d(e^{ik_y}, \alpha)^2 = 0$ . When we perturb  $\alpha$  away from 3, this root, which is quadratic for  $d(e^{ik_y}, \alpha)^2$ , will split and move into the complex plane. We look for these roots by Taylor expanding  $d(e^{i(t+is)}, \alpha)^2$  as  $s, t \rightarrow 0$  and  $\alpha \rightarrow 3$ , which gives to leading orders,

$$d(e^{i(t+is)}, \alpha)^2 \asymp (64t^2 + 128its - 64s^2 - 160t^2s^2)[1 + (\alpha - 3)] + (16 + 24t^2 + 48its - 24s^2 + 18t^2s^2)(\alpha - 3)^2. \quad (\text{S38})$$

Taking  $t = 0$  so the imaginary part of the right hand side is zero, we solve for the smallest zeros of

$$d(e^{-s}, \alpha)^2 = -64s^2 - 64s^2(\alpha - 3) + (16 - 24s^2)(\alpha - 3)^2 + O(s^3) + O((\alpha - 3)^3). \quad (\text{S39})$$

Dropping higher order terms gives that this is equal to zero for

$$s^2 = \frac{2(\alpha - 3)^3}{8 + 8(\alpha - 3) + 3(\alpha - 3)^2} = \frac{(\alpha - 3)^2}{4}(1 + O(\alpha - 3)). \quad (\text{S40})$$

Moreover, the numerator of (S36) is bounded away from zero, since  $\sin(k_y)$  has no  $\alpha$  dependence, and the other numerator terms were nonzero for  $t = s = 0$  and  $\alpha = 3$ . Thus the distance to the nearest complex zero of  $d(e^{ik_y}, \alpha)$  for  $\alpha$  near 3 is  $|s| \sim \frac{1}{2}|\alpha - 3|$ . This gives the correlation length for  $K^{-1}$  (the real-space Green's function in the free-fermion picture) along a vertical path as

$$\xi_G \sim \frac{2}{|\alpha - 3|}, \quad \text{as } \alpha \rightarrow 3, \quad (\text{S41})$$

measured in lattice distance. One could also study the correlation length along other paths similarly. We plot the inverse correlation lengths along different paths numerically in Fig. S3. In particular, this confirms (S41) numerically for the vertical path.

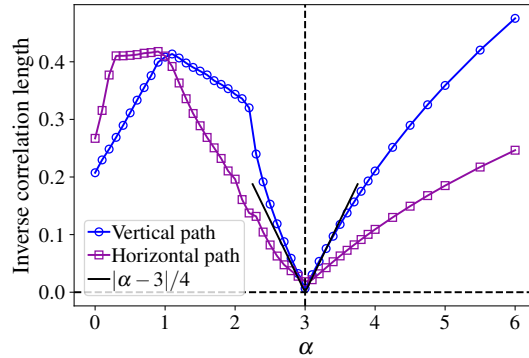


FIG. S3. Inverse correlation lengths  $\xi_G^{-1}$  for the inverse Kasteleyn matrix values  $|K^{-1}(v_0, v_\ell)|$  (or real-space Greens' function) along a vertical and horizontal path, using lattice size  $303 \times 303$ . The correlation length is calculated with respect to vertices  $v_\ell$  which include all of those in the zigzag path drawn in Fig. 3, in particular alternating between columns (for the vertical path) or rows (for the horizontal path). There are two vertices per lattice square in the zigzag path, accounting for the extra factor of  $1/2$  in the comparison to  $|\alpha - 3|/4$ . The inverse correlation lengths are calculated using a best fit regression on vertices  $\ell = 40$  to  $150$ , as measured from the center  $\ell = 0$  and ending roughly halfway to the edge at the endpoint  $\ell = 150$ .

For large  $\alpha$ , we can show along a horizontal or vertical path that

$$\xi_G \sim \frac{1}{\log\left(\frac{\alpha-1}{2}\right)}, \quad \text{as } \alpha \rightarrow \infty. \quad (\text{S42})$$

As shown in Fig. S4, the dimer-dimer inverse correlation length behaves similarly as  $\xi_{\text{dimer}} \propto \frac{1}{\log\left(\frac{\alpha-1}{2}\right)}$ . Starting from the band dispersion  $P(e^{ik_x}, e^{ik_y})$  in (S28), we see there is a complex zero at  $(k_x, k_y) = (0, i \log\left(\frac{\alpha-1}{2}\right))$ . This is also not a zero

of any of the  $Q_{st}(e^{ik_x}, e^{ik_y})$  in (S27). A quick standard estimate shows that if  $f : (\mathbb{R}/2\pi\mathbb{Z})^d \rightarrow \mathbb{C}$  has Fourier coefficients  $|\hat{f}(\xi)| \leq C e^{-\kappa \|\xi\|_2}$ , then  $f$  has analytic extension to the strip  $\{x + iv \in (\mathbb{C}/2\pi\mathbb{Z})^d : \|v\|_2 < \kappa\}$ . Thus for  $P(e^{ik_x}, e^{ik_y})$ , the complex zero prevents analytic extension to  $\kappa = \log(\frac{\alpha-1}{2})$ , which implies  $\xi_G^{-1} \leq \log(\frac{\alpha-1}{2})$ . To obtain a lower bound on  $\xi_G^{-1}$ , let  $k_x = \theta + iu$  and  $k_y = \varphi + iv$ . If  $|u| + |v| \leq \kappa = (1 - \delta) \log(\frac{\alpha-1}{2})$ , then

$$\begin{aligned} & |P(e^{i(\theta+iu)}, e^{i(\varphi+iv)})| \\ &= |e^{2i\theta} e^{-2u} + e^{-2i\theta} e^{2u} - 2 + (a - e^{-i\varphi} e^v - e^{i\theta} e^{-u} - e^{-i\theta} e^{-i\varphi} e^u e^v)(a - e^{i\varphi} e^{-v} - e^{-i\theta} e^u - e^{i\theta} e^{i\varphi} e^{-u} e^{-v})| \\ &\geq (\alpha - 3e^\kappa)^2 - 2 - 2e^{2\kappa} = \alpha^2 - O(\alpha^{2-2\delta}). \end{aligned} \quad (\text{S43})$$

As  $\alpha \rightarrow \infty$ , this is bounded away from zero. Thus there are no complex zeros of  $P$  if  $|u| + |v| \leq (1 - \delta) \log(\frac{\alpha-1}{2})$ . Then along a horizontal or vertical path, a 2-dimensional version of Lemma 2, which replaces the absolute values with the  $\ell^1$  norm [S16, Lemma 5.6], implies  $\xi_G^{-1} \geq (1 - \delta) \log(\frac{\alpha-1}{2})$  for any  $\delta > 0$  and sufficiently large  $\alpha$ .

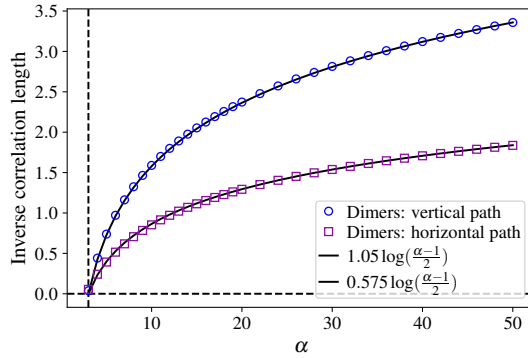


FIG. S4. Dimer-dimer inverse correlation length from  $\alpha = 3$  to 50, using lattice size  $303 \times 303$ .

For completeness, we comment on the inverse correlation lengths calculated in Fig. 5 in the Main Text. There, the inverse correlation lengths are calculated using linear regression for edge/face distances starting at 30 and ending at 150 (for dimers) or when numerical precision drops below  $10^{-15}$  (for vison correlator near  $\alpha = 1$ ).

## V. POWER-LAW DECAY AT THE CRITICAL POINT

In this section, we discuss numerics for the dimer-dimer and vison correlators at the critical point  $\alpha = 3$ . We see numerically in Fig. S5 the dimer-dimer correlator for  $\alpha = 3$  decays as a power-law, although along the horizontal path it appears to decay at a faster power than  $1/R^2$ . Note that for the square lattice at criticality, it is also known that certain pairs have dimer-dimer correlators that can decay as a power-law faster than  $1/R^2$  [S4, S18].

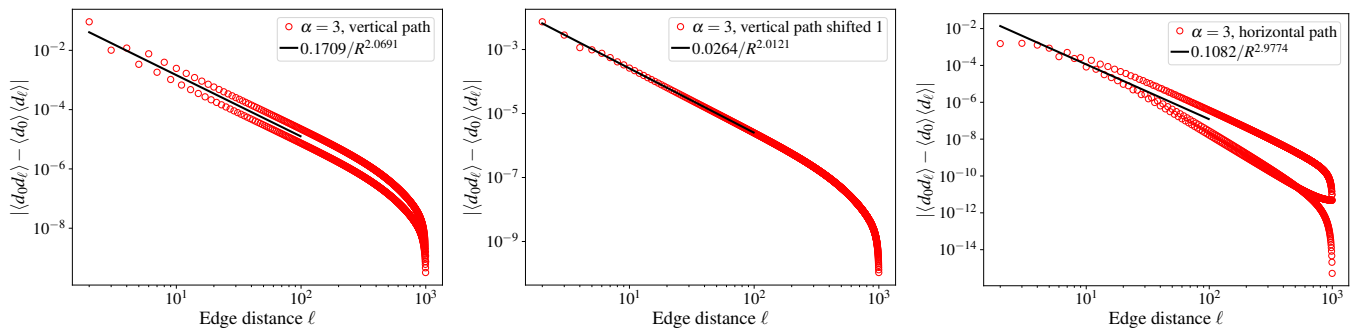


FIG. S5. Dimer-dimer correlator decay on different paths for the triangular lattice on a size  $1001 \times 1001$  grid with  $\alpha = 3$ . All plots use a log-log scale. The best fit curves  $a_1/R^{\alpha_2}$  are calculated over distances up to 100. For the vertical paths, the decay is power law  $\approx C_2/R^2$ . For the horizontal path, there appear to be different rates of decay (faster decay than  $1/R^2$  but still power-law) depending on the path index.

The vison correlator  $|\langle v_0 v_\ell \rangle|$  also decays as a power-law at criticality (Fig. S6), though determining the critical exponent  $\eta$  in the decay is difficult with only finite-size numerics. It is however plausible that one could have  $\eta = 1/4$  in agreement with the 2D Ising critical exponent, but we note the numerical values can vary depending on the region used for the linear regression. We anticipate that  $\eta$  can be determined more reliably using the infinite-size limit integrals in e.g. Eq. (S35).

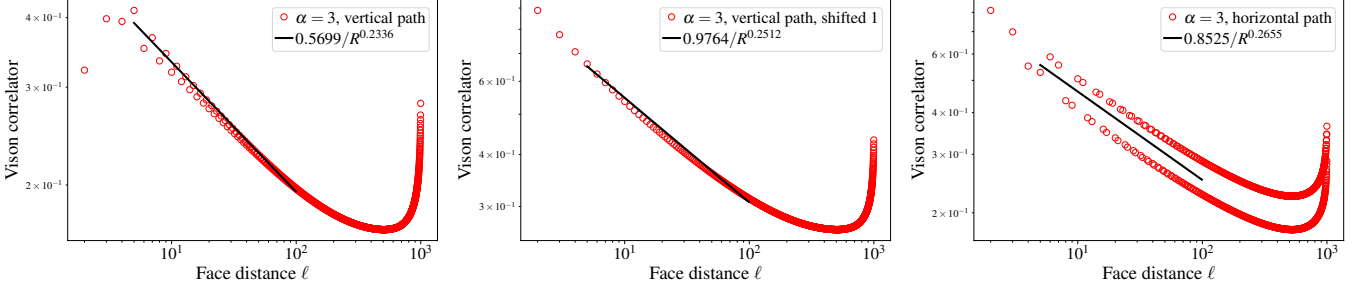


FIG. S6. Vison correlator decay at the critical value  $\alpha = 3$  for the triangular lattice on a size  $1001 \times 1001$  grid. All plots use a log-log scale. The exponent  $\eta$  in the best-fit curve  $c/R^\eta$  is somewhat sensitive to the precise region over which the curve fitting is done (here we use 5 to 100), but a value of  $\eta = 1/4$  is plausible.

## VI. CRITICAL EXPONENTS, FINITE-SIZE SCALING, AND CURVE COLLAPSE

In this section we consider the finite-size scaling shown in Fig. 6 of the Main Text along other lattice paths. There are several different types of paths:

1. Vertical path through weight  $\alpha$  horizontal edges (curve collapse shown in Main Text Fig. 6)
2. Vertical path through weight 1 horizontal edges
3. Horizontal path starting and ending in weighted faces
4. Horizontal path starting and ending in unweighted faces
5. Horizontal path starting and ending in two differently weighted faces

In Fig. S7, we consider several of these additional paths and see the curve collapse also occurs for  $\beta = 1/8$  and  $\nu = 1$ , the same as for the first case shown in the Main Text.

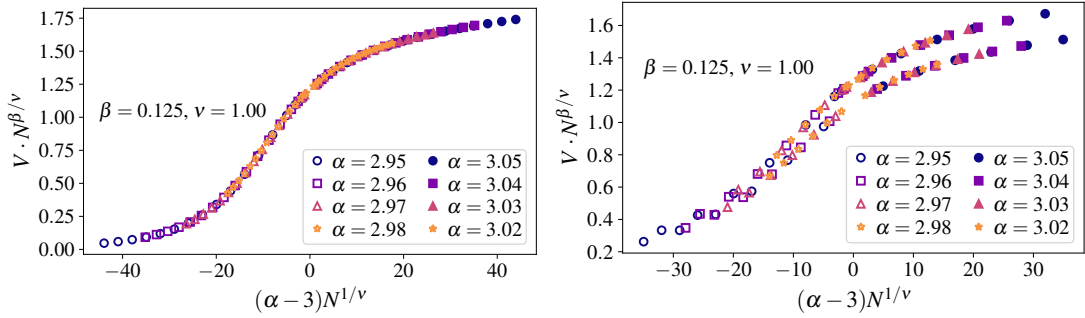


FIG. S7. (Left) Curve collapse at  $\beta = 1/8$  and  $\nu = 1$  for the vertical path through weight 1 edges, for  $N = 39, 63$  and  $99$  through  $880$  by  $60$ s. (Right) Curve collapse at  $\beta = 1/8$  and  $\nu = 1$  for horizontal paths starting in a weight 1 face, for  $N = 39, 63$ , and  $100$  through  $700$  by  $60$ s. The right figure shows two distinct curves since the path endpoint can be in a weight 1 face or weight  $\alpha$  face, depending on the value of  $N$ . One could restrict to just a single curve by choosing the values of  $N$  carefully or by shifting the path endpoint to always end in the same type of face.

We also comment why we take a square root in the finite-size scaling of  $V = \sqrt{|\langle v_0 v_\ell \rangle|}$ . For magnetization in the Ising model, one has  $\lim_{R \rightarrow \infty} \langle m(0)m(R) \rangle = \langle m \rangle^2$ , where  $\langle m \rangle$  is the average magnetization and is the order parameter. Since the

critical exponent  $\beta$  corresponds to the behavior of the order parameter rather than that of the correlator, we take the square root of the vison correlator  $|\langle v_0 v_\ell \rangle|$ .

For another comparison to the 2D Ising model, in Fig. S8 we plot  $V = \sqrt{|\langle v_0 v_\ell \rangle|}$  as a function of the weight  $\alpha$ , and observe the resulting curve closely resembles the magnetization curve for the 2D Ising model.

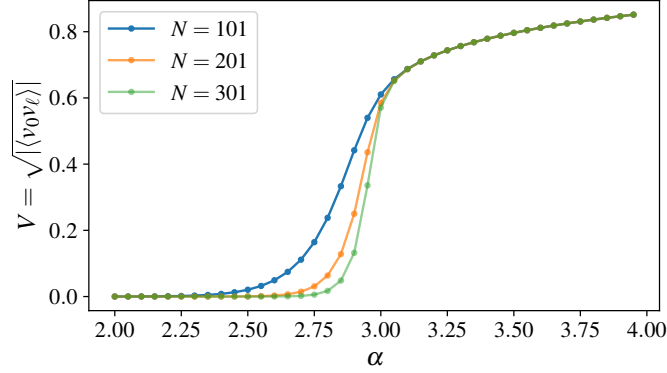


FIG. S8. Plot of  $V = \sqrt{|\langle v_0 v_\ell \rangle|}$  calculated from center halfway to the edge, for different system sizes  $N = 101, 201, 301$ . The curve resembles the magnetization curve for 2D Ising model.

## VII. DOUBLE-DIMER COVERINGS AND CONSTANT VISONS

In this section we discuss how a phase with only small loops in the double-dimer covering is related to constant vison correlator.

Let  $Z = \sum_C \mathcal{W}(C)$  be the classical partition function, where the sum is over all dimer coverings  $C$  and  $\mathcal{W}(C)$  is the classical weight assigned to the covering. Recall the vison correlator between two faces  $f_0, f_1$  is

$$\langle f_0 f_1 \rangle = \langle (-1)^{\#\text{ dimers along } \gamma} \rangle = \frac{\sum_C (-1)^{\#\text{ dimers along } \gamma} \mathcal{W}(C)}{Z}, \quad (\text{S44})$$

where  $\gamma$  is a path between  $f_0$  and  $f_1$ . We will consider double-dimer coverings  $C \cup C'$ , which consist of the edges of two independent random dimer coverings  $C$  and  $C'$ . We can write the vison correlator squared as

$$\begin{aligned} |\langle f_0 f_1 \rangle|^2 &= \frac{\sum_{C, C'} (-1)^{\#\text{ dimers in } C \cup C' \text{ along } \gamma} \mathcal{W}(C) \mathcal{W}(C')}{Z^2} \\ &= \mathbb{E}_{C, C'} [(-1)^{\#\text{ dimers in } C \cup C' \text{ along } \gamma}]. \end{aligned} \quad (\text{S45})$$

Recalling the edges in  $C \cup C'$  form only closed loops and double edges, the parity of  $\#\{\text{ dimers in } C \cup C' \text{ along } \gamma\}$  is unchanged if the path  $\gamma$  enters and exits such a loop or crosses a double edge. So the parity is only affected by loops which contain exactly one of the faces  $f_0, f_1$ . For a face  $f$ , let  $L(f) = \#\{\text{ loops in } C \cup C' \text{ that go around } f\}$ . Then

$$\begin{aligned} |\langle f_0 f_1 \rangle|^2 &= 2\mathbb{P}_{C, C'} [\#\{\text{ dimers in } C \cup C' \text{ along } \gamma\} \text{ is even}] - 1 \\ &= 2\mathbb{P}_{C, C'} [L(f_0) \text{ and } L(f_1) \text{ have the same parity}] - 1. \end{aligned} \quad (\text{S46})$$

If the loops in  $C \cup C'$  are all small, such as seen in the ordered phase in the right-mode part of Fig. 1, then this suggests that  $L(f)$  should be a local quantity since it only involves nearby dimers in the small loops. Then  $L(f_0)$  and  $L(f_1)$  should be nearly independent for far apart faces due to exponential decay of dimer correlations, giving

$$\begin{aligned} |\langle f_0 f_1 \rangle|^2 &= 2(\mathbb{P}[L(f_0), L(f_1) \in 2\mathbb{N}] + \mathbb{P}[L(f_0), L(f_1) \notin 2\mathbb{N}]) - 1 \\ &\approx 2\mathbb{P}[L(f_0) \in 2\mathbb{N}]\mathbb{P}[L(f_1) \in 2\mathbb{N}] + 2\mathbb{P}[L(f_0) \notin 2\mathbb{N}]\mathbb{P}[L(f_1) \notin 2\mathbb{N}] - 1 + O(e^{-cn}). \end{aligned} \quad (\text{S47})$$

Letting  $p_0 = \mathbb{P}[L(f_0) \in 2\mathbb{N}]$  and  $p_1 = \mathbb{P}[L(f_1) \in 2\mathbb{N}]$ , this becomes

$$\begin{aligned} |\langle f_0 f_1 \rangle|^2 &\approx 2(p_0 p_1 + (1 - p_0)(1 - p_1)) - 1 + O(e^{-cn}) \\ &= 4p_0 p_1 - 2p_0 - 2p_1 + 1 + O(e^{-cn}). \end{aligned} \quad (\text{S48})$$

To have this tend to 0 as the distance between the faces goes to  $\infty$ , we need  $p_0 = 1/2$  or  $p_1 = 1/2$ . If we want the vison correlator to go to 0 for all paths, then by using periodicity to consider  $f_0$  and  $f_1$  the same type of face, we must have  $p := \mathbb{P}[L(f) \in 2\mathbb{N}] = 1/2$  for all faces  $f$  (in the infinite size limit). Due to gauge equivalence of edge weights [S19, S20], non-uniform edge weights is equivalent to non-uniform face weights. If we have different face weights, or even different face shapes for more complicated lattices, it seems unlikely that we could have all faces have the exact same probability  $p_0 = 1/2$ . For example, with varying face weights, some faces are likely to have a different average number of edges around them than other faces. Additionally, the condition  $p_0 = p_1 = 1/2$  seems very unstable to perturbations. Overall, the above suggests that we will not have a topological spin liquid phase or vison decay if the double-dimer coverings have only small loops.

We conjecture, due to the square-octagon example [S13] and related general double-dimer properties of bipartite lattices [S12], that it may then be the case that periodic bipartite lattices cannot host a  $\mathbb{Z}_2$  quantum spin liquid phase. We emphasize this is a different suggested reasoning than the conventional argument for lack of spin liquid at the RK point on bipartite lattices [S21–S23], which argues that such (unweighted) models should be critical. However, this cannot hold for bipartite lattices in general, as the unweighted square-octagon lattice is bipartite but exhibits exponential decay of dimer-dimer correlators.

- 
- [S1] I. Hartarsky, L. Lichev, and F. L. Toninelli, Local dimer dynamics in higher dimensions, *Ann. Inst. Henri Poincaré Comb. Phys. Interact.* **10.4171/AIHPD/200** (2024), published online 26 August 2024.
- [S2] C. Kenyon and E. Rémila, Perfect matchings in the triangular lattice, *Discrete Math.* **152**, 191 (1996).
- [S3] P. W. Kasteleyn, The statistics of dimers on a lattice: I. the number of dimer arrangements on a quadratic lattice, *Physica* **27**, 1209 (1961).
- [S4] R. Kenyon, Lectures on Dimers (2009), [arXiv:0910.3129](https://arxiv.org/abs/0910.3129).
- [S5] D. Cimasoni, The geometry of dimer models, *Winter Braids Lect. Notes* **1**, Exp. No. 2, 14 (2014).
- [S6] V. Gorin, *Lectures on random lozenge tilings*, Cambridge Studies in Advanced Mathematics, Vol. 193 (Cambridge University Press, Cambridge, 2021) pp. viii+250.
- [S7] P. W. Kasteleyn, Graph theory and crystal physics, in *Graph Theory and Theoretical Physics*, edited by F. Harary (Academic Press, London, 1967) pp. 43–110.
- [S8] P. Fendley, R. Moessner, and S. L. Sondhi, Classical dimers on the triangular lattice, *Phys. Rev. B* **66**, 214513 (2002).
- [S9] One could alternatively define a Kasteleyn orientation in terms of clockwise orientation.
- [S10] R. Kenyon, Conformal invariance of loops in the double-dimer model, *Comm. Math. Phys.* **326**, 477 (2014).
- [S11] D. Cimasoni and N. Reshetikhin, Dimers on surface graphs and spin structures. I, *Comm. Math. Phys.* **275**, 187 (2007).
- [S12] R. Kenyon, A. Okounkov, and S. Sheffield, Dimers and amoebae, *Ann. of Math. (2)* **163**, 1019 (2006).
- [S13] J. Shah, L. Shou, J. Shuler, and V. Galitski, Breakdown of the thermodynamic limit in quantum spin and dimer models, [arXiv preprint arXiv:2506.15769](https://arxiv.org/abs/2506.15769) (2025).
- [S14] H. Cohn, R. Kenyon, and J. Propp, A variational principle for domino tilings, *J. Amer. Math. Soc.* **14**, 297 (2001).
- [S15] If  $z \in \{-1, \alpha\}$ , then  $c_1(z, \alpha) = 0$  and the denominator is simply linear with a zero at  $w = -c_3(z, \alpha)/c_2(z, \alpha) = 0$ . The contour integral over  $w$  is then zero for  $\ell, j \neq 0$ , which agrees with the formulas (S35) and (S36) for  $z \neq -1, \alpha$ .
- [S16] H. Broer and F. Takens, *Dynamical systems and chaos*, Applied Mathematical Sciences, Vol. 172 (Springer, New York, 2011) pp. xvi+313.
- [S17] V. I. Arnol'd, *Geometrische Methoden in der Theorie der gewöhnlichen Differentialgleichungen* (Birkhäuser Verlag, Basel, 1987) p. 320, translated from the Russian by Ernst Günter Giessmann, Bernd Graw and Horst Theel.
- [S18] M. E. Fisher and J. Stephenson, Statistical mechanics of dimers on a plane lattice. II. dimer correlations and monomers, *Phys. Rev.* **132**, 1411 (1963).
- [S19] R. Kenyon, Height fluctuations in the honeycomb dimer model, *Comm. Math. Phys.* **281**, 675 (2008).
- [S20] C. Boutillier, D. Cimasoni, and B. de Tilière, Minimal bipartite dimers and higher genus Harnack curves, *Probab. Math. Phys.* **4**, 151 (2023).
- [S21] C. L. Henley, Relaxation time for a dimer covering with height representation, *J. Statist. Phys.* **89**, 483 (1997).
- [S22] E. Fradkin, D. A. Huse, R. Moessner, V. Oganesyan, and S. L. Sondhi, Bipartite Rokhsar–Kivelson points and cantor deconfinement, *Phys. Rev. B* **69**, 224415 (2004).
- [S23] R. Moessner and K. S. Raman, Quantum dimer models, in *Introduction to Frustrated Magnetism: Materials, Experiments, Theory* (Springer Berlin Heidelberg, Berlin, Heidelberg, 2011) pp. 437–479.